



# Effect of Sintering Temperature on the Microstructural Evolution of ZnO Varistors

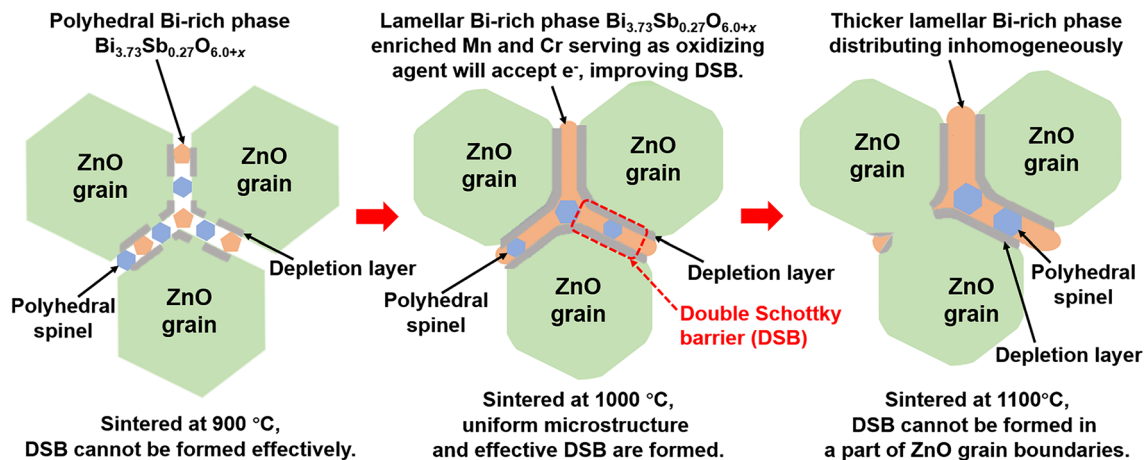
Wenbin Cao<sup>1</sup> · Yuwei Guo<sup>1</sup> · Jinfeng Su<sup>1</sup> · Jianke Liu<sup>1</sup>

Received: 6 September 2022 / Accepted: 24 October 2022 / Published online: 28 November 2022  
© The Minerals, Metals & Materials Society 2022

## Abstract

The effect of sintering temperature on the microstructural evolution and electrical properties of ZnO-Bi<sub>2</sub>O<sub>3</sub>-Sb<sub>2</sub>O<sub>3</sub>-MnO<sub>2</sub>-Co<sub>2</sub>O<sub>3</sub>-Cr<sub>2</sub>O<sub>3</sub>-SiO<sub>2</sub> varistors was studied in detail. With sintering at 900°C, polyhedral Bi-rich phase Bi<sub>3.73</sub>Sb<sub>0.27</sub>O<sub>6.0+x</sub> was distributed in the ZnO grain boundaries, preventing the effective formation of the double Schottky barrier. With an increase in the sintering temperature from 900°C to 1000°C, the liquefaction of Bi-rich phase occurred, leading to the beneficiation of Mn and Cr in the Bi-rich phase Bi<sub>3.73</sub>Sb<sub>0.27</sub>O<sub>6.0+x</sub>, and a lamellar Bi-rich phase formed in the ZnO grain boundaries during cooling. Excess O and enriched Mn<sup>4+</sup> in Bi-rich phase Bi<sub>3.73</sub>Sb<sub>0.27</sub>O<sub>6.0+x</sub> serving as oxidizing agent acted as acceptors of e<sup>-</sup>, thus improving the double Schottky barrier. When the sintering temperature was further increased from 1000°C to 1100°C, the volatilization of the Bi-rich phase intensified, the thickness of the Bi-rich thin layers increased, and the uniformity decreased, leading to the deterioration of the microstructure and electrical properties of the ZnO varistors. Ion diffusion was stronger for the samples sintered at higher temperature, leading to more obvious polarization and loss peak. Finally, the ZnO varistors sintered at 1000°C for 2 h obtained a nonlinear coefficient of 43.4 ± 2.3, voltage gradient of 451 ± 4 V/mm, and leakage current density of 4.5 ± 0.4 μA/cm<sup>2</sup>, demonstrating optimal microstructural uniformity and reproducibility of the sample preparation. The intensive study of sintering temperature has important relevance for the preparation of ZnO varistors with excellent microstructural uniformity and electrical properties.

## Graphical Abstract



**Keywords** ZnO varistor · sintering temperature · microstructural evolution · electrical property

✉ Wenbin Cao  
caowenbin@sust.edu.cn

<sup>1</sup> Research Center for Semiconductor Materials and Devices,  
Shaanxi University of Science and Technology,  
Xi'an 710021, China

## Introduction

ZnO varistors are usually used as the core element in the manufacture of surge arresters because of their outstanding nonlinear electric field–current density ( $E$ – $J$ ) characteristics and energy surge absorption capability.<sup>1–3</sup> To manufacture ZnO varistor ceramics, ZnO is used as the main ingredient to form the basic microstructure, Bi<sub>2</sub>O<sub>3</sub> (or Pr<sub>6</sub>O<sub>11</sub>) is used as the requisite ingredient to form the double Schottky barrier in the ZnO grain boundaries, and other minor oxide additives (such as Cr<sub>2</sub>O<sub>3</sub>, MnO<sub>2</sub>, Sb<sub>2</sub>O<sub>3</sub>, Co<sub>2</sub>O<sub>3</sub>, and SiO<sub>2</sub>) are typically used to improve the microstructure and electrical properties.<sup>4–6</sup>

The ZnO varistor is connected in parallel with an electronic device to protect the device.<sup>2</sup> The nonlinear coefficient reflects the response speed and the leakage current reflects the thermal loss level, which are the key electrical performance parameters for ZnO varistors.<sup>2</sup> Doping is the most effective means of improving the electrical properties. He et al. conducted in-depth studies on the impacts of doping (In,<sup>4</sup> Al,<sup>7</sup> Ga,<sup>8</sup> or Co<sup>9</sup>) on the structure and electrical properties of ZnO varistors. Doping with other elements (such as Cr,<sup>5</sup> Ni,<sup>5</sup> Y,<sup>5</sup> Bi,<sup>10</sup> Si,<sup>11,12</sup> B,<sup>13</sup> or Ca<sup>14</sup>) has also been used to improve the electrical properties. Doping will change the donor density in the interior of ZnO grains, improve the microstructures of Bi-rich and spinel phases, and further improve the characteristic of the double Schottky barrier, leading to a larger nonlinear coefficient and smaller leakage current.<sup>11,12,14</sup> The sintering method also has important effects on the structure and electrical properties of ZnO varistors. Rapid sintering techniques (such as flash sintering,<sup>15,16</sup> microwave sintering,<sup>17</sup> and spark plasma sintering<sup>18,19</sup>) have been used to prepare ZnO varistors. Defect distribution and double Schottky barrier features have important effects on the electrical properties of ZnO varistors, but the tuning and control of defects is difficult with rapid sintering techniques.<sup>1</sup> ZnO varistors are usually sintered by conventional pressureless sintering, and the sintering parameters (temperature,<sup>20</sup> rate,<sup>21</sup> pre-calcination,<sup>22</sup> two-step sintering,<sup>23</sup> and so on) affect the grain growth and relative density, which will further affect the microstructure and nonlinear  $E$ – $J$  characteristics. Various studies have investigated the effects of sintering temperature on Zn–Bi–O,<sup>20</sup> Zn–Bi–Sb–Co–Ca–O,<sup>24</sup> Zn–V–Mn–O,<sup>25</sup> Zn–Pr–Dy–Co–Cr–Si–O,<sup>26</sup> Zn–Pr–Co–Cr–Y–Al–O,<sup>27</sup> Zn–Bi–Sb–Mn–Co–Cr–O,<sup>28</sup> Zn–Bi–Mn–Co–B–O,<sup>29</sup> and Zn–Bi–Sb–Mn–Co–O<sup>30</sup> varistors, which revealed that the sintering temperature affects the phase evolution, the distribution of defects and Bi-rich phase, and the characteristics of the double Schottky barrier, resulting in obvious differences in electrical properties with different sintering temperatures.<sup>24–31</sup> Zn–Bi–Sb–Mn–Co–Cr–Si–O is

an important basic component for preparing ZnO varistors, but detailed studies examining the microstructural evolution with sintering temperature are lacking.<sup>1,4,7–9</sup> Meanwhile, the electrical properties of ZnO varistor samples prepared with the same experimental conditions often differ among different batches.

In this work, the effect of sintering temperature on the structure and electrical properties of ZnO–Bi<sub>2</sub>O<sub>3</sub>–Sb<sub>2</sub>O<sub>3</sub>–MnO<sub>2</sub>–Co<sub>2</sub>O<sub>3</sub>–Cr<sub>2</sub>O<sub>3</sub>–SiO<sub>2</sub> varistors was investigated. The elemental distribution, phase distribution, grain boundary evolution, and double Schottky barrier were analyzed, and the standard deviations of the nonlinear coefficient, voltage gradient, and leakage current for the samples prepared more than three times were analyzed.

## Experimental Procedure

ZnO varistors were prepared with the same components of 95.05 mol.% ZnO, 0.7 mol.% Bi<sub>2</sub>O<sub>3</sub>, 1.0 mol.% Sb<sub>2</sub>O<sub>3</sub>, 0.5 mol.% MnO<sub>2</sub>, 0.5 mol.% Cr<sub>2</sub>O<sub>3</sub>, 1.0 mol.% Co<sub>2</sub>O<sub>3</sub>, and 1.25 mol.% SiO<sub>2</sub>. First, all of the raw powders mixed with ultrapure water were ball-milled at a rate of 500 r/min for 3 h. After drying and grinding, the powder obtained was mixed with 0.8 wt.% polyvinyl alcohol (PVA) by ball milling. The dry particles were pressed at 468 MPa into green pellets 8 mm in diameter and 1.5 mm thick. The green pellets were heated to 600°C for 5 h to remove organic matter, followed by heating at a rate of 3°C/min to 900–1100°C for 2 h, and then cooled naturally to room temperature. The ZnO varistor samples were obtained. In order to test the electrical properties, the upper and lower surfaces of the ZnO varistor samples were coated with silver paste and heated to 600°C for 30 min.

X-ray diffraction (XRD, Rigaku D/Max-2200 PC diffractometer, Japan) was used to analyze the crystal structure of the ZnO varistor samples. To analyze the microstructure and clearly observe the Bi-rich phase, the fracture surfaces of the ZnO varistors were analyzed by scanning electron microscopy (SEM, Zeiss SUPRA 55-VP, Germany), with further analysis by energy-dispersive spectroscopy (EDS). The mean grain size was statistically calculated from more than 500 ZnO grains observed in different areas of different SEM images. The  $E$ – $J$  characteristics of the ZnO varistors were tested by a source measure (Keithley 2410 SourceMeter, USA). The nonlinear coefficient  $\alpha$  was determined as follows:  $\alpha = 1/\log(E_2/E_1)$ , and the electric fields  $E_1$  and  $E_2$  were obtained at current of 0.1 and 1.0 mA/cm<sup>2</sup>, respectively. The voltage gradient  $E_{1\text{mA}}$  was obtained at current of 1.0 mA/cm<sup>2</sup>, while the leakage current density  $J_L$  was determined at an electric field of 0.75  $E_{1\text{mA}}$ . The capacitance–voltage ( $C$ – $V$ ) characteristics were analyzed using a dielectric impedance spectrometer (Concept 43, Novocontrol

Technologies, Germany). The relative dielectric constant  $\epsilon_r$  and dissipation factor  $\tan\delta$  were tested using a capacitance meter (Hioki IM3536, Japan). The sample experiments were carried out more than three times, and the mean values and standard deviations were calculated as the values of  $\alpha$ ,  $E_{1mA}$ , and  $J_L$ ; the other characterizations were performed using the samples with values of  $\alpha$ ,  $E_{1mA}$ , and  $J_L$  close to the mean values.

## Results and Discussion

The ZnO varistor samples obtained at different sintering temperatures of 900°C, 950°C, 1000°C, 1050°C, and 1100°C were analyzed using XRD, and the XRD patterns are shown in Fig. 1. The samples obtained at different sintering

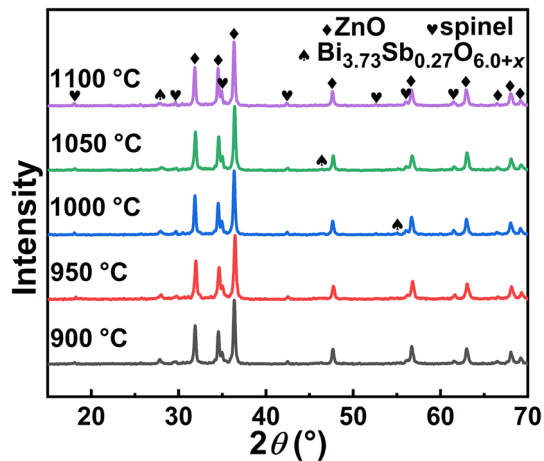
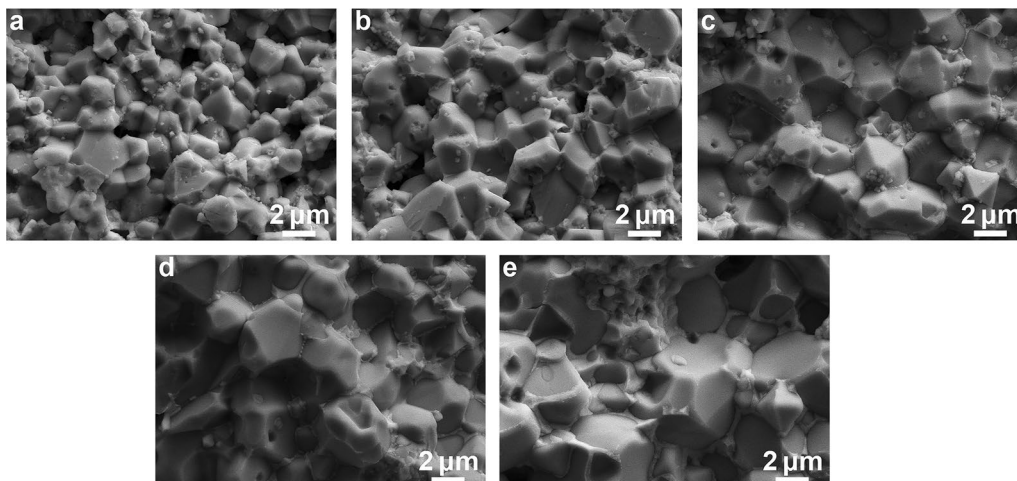


**Fig. 1** The XRD patterns of the ZnO varistor samples obtained at different sintering temperatures.

temperatures show similar diffraction patterns, in which ZnO is the main phase (JCPDS No. 89-0511), while some weak diffraction peaks corresponding to spinel and Bi-rich phase  $\text{Bi}_{3.73}\text{Sb}_{0.27}\text{O}_{6.0+x}$  (JCPDS No. 44-0191) are observed, which is consistent with the typical phase composition of ZnO-Bi<sub>2</sub>O<sub>3</sub>-based varistors.<sup>2,3,5,32</sup> The diffraction peaks of  $\text{Co}_{2.33}\text{Sb}_{0.67}\text{O}_4$  (JCPDS No. 15-0517),  $\text{Zn}_{2.33}\text{Sb}_{0.67}\text{O}_4$  (JCPDS No. 15-0687),  $\text{Mn}_{1.50}\text{Cr}_{1.25}\text{Sb}_{0.25}\text{O}_4$  (JCPDS No. 39-0027), and  $\text{Mn}_{1.20}\text{Cr}_{1.70}\text{Sb}_{0.10}\text{O}_4$  (JCPDS No. 39-0028) correspond to the diffraction peaks of spinel phase shown in Fig. 1. This reveals that Sb is the main element present in the Bi-rich and spinel phases formed during sintering.

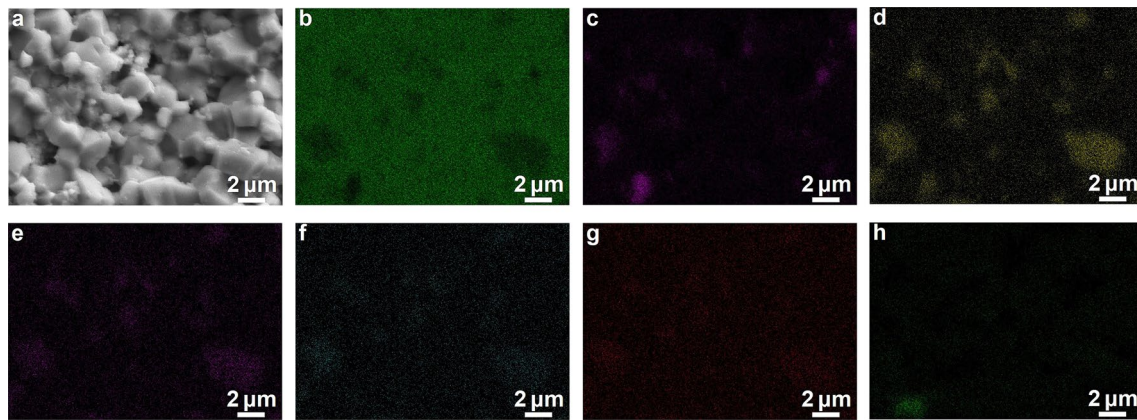
To further analyze the microstructure, the ZnO varistors were tested by SEM and EDS. Figure 2 shows the SEM images of the samples obtained at different sintering temperatures. With sintering at 900°C for 2 h, pores are clearly distributed in the sample. The pores decrease with an increase in sintering temperature to 950°C. With sintering temperatures of 1000–1100°C, few pores are observed, and densification is basically achieved.

Figure 3 shows the SEM image and related EDS mapping of the ZnO varistor sample obtained with sintering at 900°C for 2 h. It reveals that Co is distributed uniformly in the sample, with the other elements aggregated in some areas and uniformly distributed in other areas. The distribution of Zn is complementary to the distribution of Sb. The distribution of Bi is completely involved in the distribution of Sb, and Sb is distributed more extensively, while Bi/Sb-rich areas have a polygon shape. Cr and Mn are aggregated in the Sb-rich areas, but are not aggregated in the Bi-rich areas. Si is uniformly distributed on the whole, but a small amount of Si is enriched as a new phase which is difficult to observe in the XRD patterns in Fig. 1. The other elements are not enriched in the Si-enriched areas, so the Si-enriched areas



**Fig. 2** SEM images of the ZnO varistor samples prepared at different sintering temperatures of 900°C (a), 950°C (b), 1000°C (c), 1050°C (d), and 1100°C (e).





**Fig. 3** The SEM image (a) and related EDS mapping of Zn (b), Bi (c), Sb (d), Cr (e), Mn (f), Co (g), and Si (h) of the ZnO varistor sintered at 900°C.

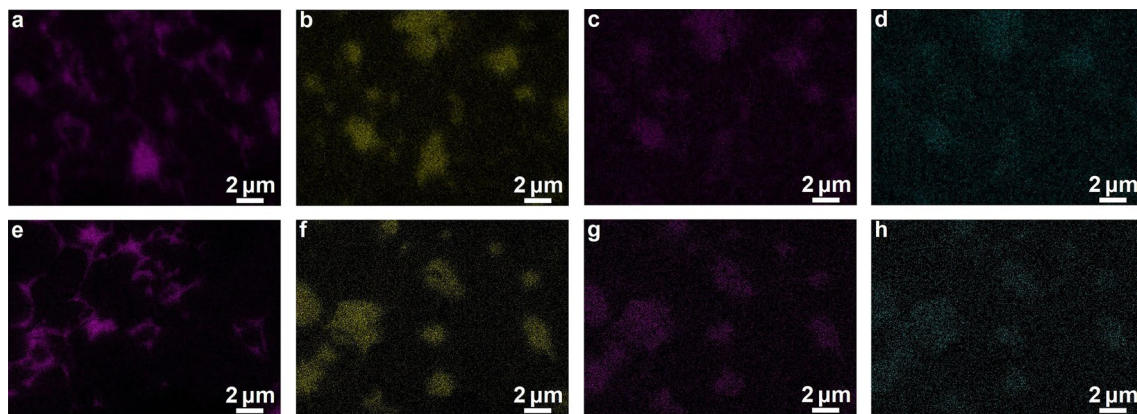


**Fig. 4** EDS mapping of Bi (a), Sb (b), Cr (c), and Mn (d) of the ZnO varistor sintered at 1000°C and EDS mapping of Bi (e), Sb (f), Cr (g), and Mn (h) of the ZnO varistor sintered at 1100°C.

may correspond to  $\text{SiO}_2$ . The ZnO varistor samples sintered at 1000 and 1100°C for 2 h were also analyzed by EDS, and the EDS maps are shown in Fig. 4 (the distribution of Co and Si for the samples sintered at 1000°C and 1100°C is the same as that in Fig. 3 and is not shown in Fig. 4). Compared with the EDS mapping in Fig. 3, Fig. 4 shows that a part of Bi-rich areas have a polygon shape, whereas the other Bi-rich areas have a banded distribution, while Mn and Cr are aggregated in the Sb-rich and Bi-rich areas for the ZnO varistor samples sintered at 1000 or 1100°C.

According to the above XRD patterns, SEM images, and EDS mapping, the main grains in Fig. 2 are ZnO, in which traces of Bi, Sb, Co, Cr, Mn, and Si exist, and the mean size of ZnO grains increases from 2.0  $\mu\text{m}$  to 4.8  $\mu\text{m}$  with an increase in the sintering temperature from 900°C to 1100°C (shown in Table I). The Bi-rich areas in Figs. 3 and 4 are mainly Bi-rich phase  $\text{Bi}_{3.73}\text{Sb}_{0.27}\text{O}_{6.0+x}$ . With sintering at 900°C, a Bi-rich phase with polyhedral shape exists in the ZnO grain boundaries. With sintering at 950°C, a

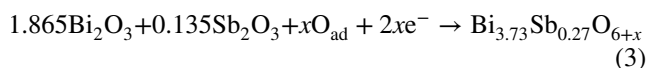
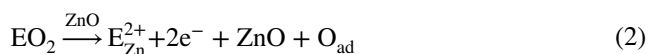
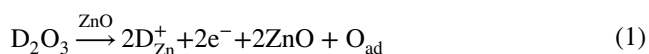
**Table I** The microstructural and electrical parameters of the ZnO varistors obtained at different temperatures

Sintering temperature (°C)	$d$ ( $\mu\text{m}$ )	$\varphi_b$ (eV)	$\alpha$	$E_{1\text{mA}}$ (V/mm)	$J_L$ ( $\mu\text{A}/\text{cm}^2$ )
900	2.02	3.8	$13.6 \pm 1.1$	$943 \pm 21.7$	$45.6 \pm 4.6$
950	2.81	4.2	$19.8 \pm 2.9$	$558 \pm 26.8$	$36.4 \pm 8.7$
1000	3.94	4.8	$43.4 \pm 2.3$	$451 \pm 3.8$	$4.5 \pm 0.4$
1050	4.06	4.1	$31.3 \pm 2.5$	$409 \pm 9.2$	$29.3 \pm 31.7$
1100	4.80	2.2	$8.1 \pm 2.6$	$342 \pm 29.7$	$112.6 \pm 72.1$

lamellar Bi-rich phase appears, confirming the formation of Bi-rich liquid phase during sintering. The Bi-rich liquid phase formed during sintering wets the ZnO grain boundaries, and a segregation layer containing Bi and other ions forms during cooling, resulting in the formation of the double Schottky barrier.<sup>2</sup> With sintering at 1000°C, a mass of lamellar Bi-rich phase is distributed uniformly in the

ZnO grain boundaries. The thickness of the lamellar Bi-rich phase increases with increased sintering temperature, but the uniformity worsens when the sintering temperature exceeds 1000°C. The Bi-rich phase is mainly composed of Bi and Sb, but Cr and Mn aggregate in the interior of the Bi-rich phase when the sintering temperature is larger than 1000°C, which may be because the liquefaction of Bi<sub>2</sub>O<sub>3</sub> improves the solid solubility of Cr and Mn in Bi-rich phase. The spinel phase distributed in the ZnO grain boundary has a polyhedral shape throughout, in which Sb is the main element. Cr and Mn are also aggregated in the interior of the spinel phase, and the content of Cr and Mn increase with increased sintering temperature. A trace of SiO<sub>2</sub> exists as a single phase, and Co is distributed uniformly throughout the samples, which is consistent with our previous research on ZnO-Pr<sub>6</sub>O<sub>11</sub>-based varistors.<sup>33</sup>

A mass of Sb and a trace of Cr and Mn dissolve in the Bi<sub>2</sub>O<sub>3</sub> liquid phase during sintering, and a lamellar Bi-rich solid phase appears between the ZnO grains during cooling. Combined with the XRD and EDS analyses, the Bi-rich phase mainly has the form of Bi<sub>3.73</sub>Sb<sub>0.27</sub>O<sub>6.0+x</sub>. The mainly reactions during sintering can be described as follows<sup>13,34</sup>:



where D mainly represents Co or Cr, and E represents Mn or Si. The chemical formula for the stoichiometric ratio is Bi<sub>3.73</sub>Sb<sub>0.27</sub>O<sub>6.0</sub>, so excess O exists in the phase of Bi<sub>3.73</sub>Sb<sub>0.27</sub>O<sub>6.0+x</sub>. According to the EDS analysis, Mn, Cr, Co, and Si acting as donor impurities distributed in the ZnO grains will undergo defect reactions as described in Eqs. 1 and 2 during sintering.<sup>13,34</sup> Therefore, point defects of D<sub>Zn</sub><sup>+</sup>, E<sub>Zn</sub><sup>2+</sup>, and e<sup>-</sup> will exist, leading to ZnO grains having N-type properties, while acceptor defects O<sub>ad</sub> are distributed in the ZnO grains. Bi-rich phase Bi<sub>3.73</sub>Sb<sub>0.27</sub>O<sub>6.0</sub> distributed in the ZnO grain boundaries forms a space network, providing an important path for O<sub>ad</sub> transport.<sup>2,11,35</sup> Thus, Bi<sub>3.73</sub>Sb<sub>0.27</sub>O<sub>6.0</sub> will more readily accept abundant O<sub>ad</sub> and e<sup>-</sup> from the ZnO grains, and electronegative Bi<sub>3.73</sub>Sb<sub>0.27</sub>O<sub>6.0+x</sub> thin layers will form. The free electrons near the ZnO grain boundaries will be exhausted, while the electropositive D<sub>Zn</sub><sup>+</sup> and E<sub>Zn</sub><sup>2+</sup> will remain,<sup>11,36</sup> thus resulting in the formation of a double Schottky barrier. Meanwhile, Mn<sup>4+</sup> aggregated in Bi-rich phase will partially serve as an oxidizing agent to accept e<sup>-</sup>, which will increase the barrier height.<sup>37</sup>

The double Schottky barriers form due to the distribution of Bi-rich phase in the ZnO grain boundaries, further

influencing the electrical properties of the ZnO varistors. The C–V characteristics of the ZnO varistors obtained at different temperatures are shown in Fig. 5. The capacitance as a function of voltage is determined as follows<sup>12,38</sup>:

$$\left(\frac{1}{C} - \frac{1}{2C_0}\right)^2 = \frac{2(\varphi_b + V_{gb})}{qN_d\epsilon} \quad (4)$$

where C is the capacitance of the unit area of a grain boundary, C<sub>0</sub> is the value of C at V<sub>gb</sub>=0 V, φ<sub>b</sub> is the double Schottky barrier height, V<sub>gb</sub> is the applied voltage per grain boundary, ε is the permittivity of the ZnO grains, q is the electronic charge, and N<sub>d</sub> is the donor density in the ZnO grains. By testing the relationship between macroscopic capacitance and applied voltage while considering the diameter, thickness, and average grain size of the ZnO varistor samples, the value of φ<sub>b</sub> can be calculated according to the slope and intercept of the line of (1/C – 1/C<sub>0</sub>)<sup>2</sup> versus V<sub>gb</sub>, which is shown in Table I. The barrier height φ<sub>b</sub> increases from 3.8 eV to 4.8 eV with the increase in sintering temperature from 900°C to 1000°C, and then decreases with higher temperature, which is because the Bi-rich phase including a mass of defects is distributed more uniformly in the ZnO grain boundaries for the ZnO varistor sintered at 1000°C.<sup>24</sup>

The microstructure determines the electrical properties. Figure 6 shows the E–J curves of the ZnO varistors sintered at different temperatures. The nonlinear coefficient α, voltage gradient E<sub>1mA</sub>, and the leakage current density J<sub>L</sub> calculated according to the E–J curve are listed in Table I. The value of α increases with the increase in temperature from 900°C to 1000°C, and then decreases with a further increase in temperature from 1000°C to 1100°C. The variation trend of the leakage current density J<sub>L</sub> with increasing temperature is contrary to that of the nonlinear

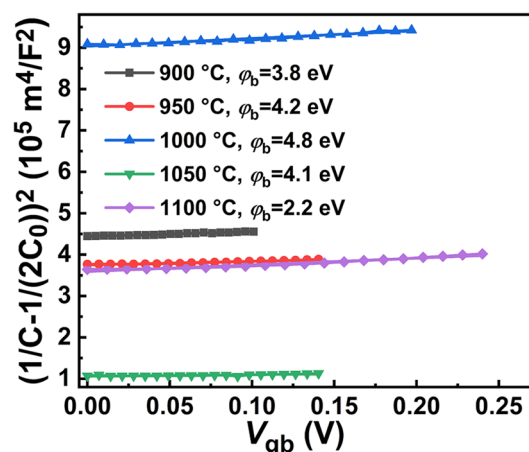


Fig. 5 The C–V characteristics of the ZnO varistors obtained at different temperatures.

coefficient. The voltage gradient  $E_{1mA}$  always decreases with increasing sintering temperature.

With sintering at 900°C for 2 h, the densification of the ZnO varistor sample was incomplete, and the Bi-rich phase  $\text{Bi}_{3.73}\text{Sb}_{0.27}\text{O}_{6.0+x}$  mainly retained a solid state during sintering, with a polyhedral shape and distributed in the ZnO grain boundaries, resulting in the inability to effectively form a double Schottky barrier. The value of the nonlinear coefficient  $\alpha$  was only 13.6, the leakage current density  $J_L$  had a larger value of  $45.6 \mu\text{A}/\text{cm}^2$ , and the voltage gradient  $E_{1mA}$  had a maximum value of 943 V/mm because the ZnO varistor sintered at 900°C had a smaller mean grain size of 2.0  $\mu\text{m}$ . With an increase in sintering temperature from 900°C to 1000°C, the Bi-rich liquid phase mainly dissolving Sb, Mn, and Cr formed during sintering, and Bi-rich thin layers were distributed between the ZnO grains formed during cooling, leading to the formation of high-quality double Schottky barriers.<sup>2</sup>

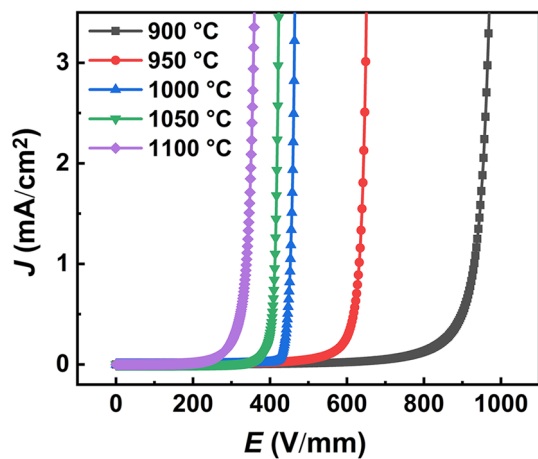


Fig. 6 The  $E$ - $J$  characteristics of the ZnO varistors obtained at different temperatures.

Therefore, the nonlinear coefficient  $\alpha$  increased while the leakage current density  $J_L$  decreased with the increase in temperature from 900°C to 1000°C. When the temperature was further increased from 1000°C to 1100°C, the volatilization of Bi-rich phase intensified, and the thickness of the Bi-rich thin layers clearly increased, leading to lower uniformity of the Bi-rich thin layers.<sup>24,28</sup> As a result, the double Schottky barriers were not distributed equally and could not be formed effectively in a part of the ZnO grain boundaries, leading to a decrease in the nonlinear coefficient  $\alpha$  and an increase in the leakage current density  $J_L$  with an increase in the sintering temperature from 1000°C to 1100°C. The microstructural evolution of the ZnO varistors with increasing sintering temperature is summarized in Fig. 7. The voltage gradient  $E_{1mA}$  decreased with increased temperature due to the increase in the mean grain size.<sup>27</sup> The barrier height  $\phi_b$  demonstrates a similar change trend as the nonlinear coefficient  $\alpha$ , which is consistent with the equation  $\alpha = (\nu/E)\phi_b^{3/2}$ , where  $\nu$  is a constant and  $E$  is the electric field intensity.<sup>11,35</sup> For Zn-Bi-Sb-Co-Ca-O,<sup>24</sup> Zn-Bi-Sb-Mn-Co-Cr-O,<sup>28</sup> and Zn-Bi-Mn-Co-B-O<sup>29</sup> varistors, the best sintering temperatures with the optimal nonlinear properties were 1050°C, 1150°C, and 1100°C, respectively. In this work, the optimal sintering temperature is 1000°C, which is lower than that in the above-mentioned literature,<sup>24,28,29</sup> attributed to the fact that SiO<sub>2</sub> doping reduces the sintering temperature.<sup>12</sup>

The standard deviation calculated for the samples prepared more than three times are listed in Table I. With sintering at 1000°C, the values of  $\alpha$ ,  $J_L$ , and  $E_{1mA}$  had the lowest standard deviation in total. With sintering at higher or lower temperature, the standard deviation increased. Therefore, the samples sintered at 1000°C demonstrated optimal microstructural uniformity and reproducibility of sample preparation. Finally, the ZnO varistor sample obtained at 1000°C for 2 h showed a nonlinear coefficient

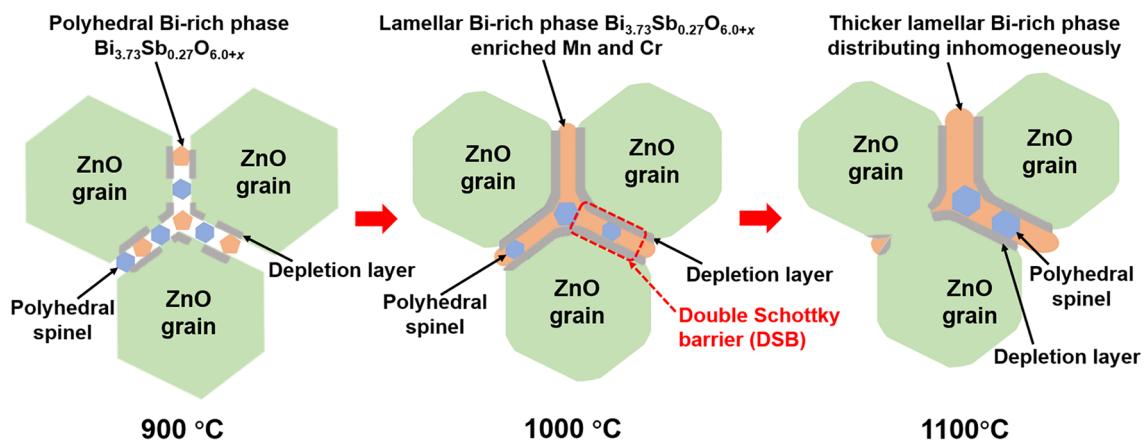
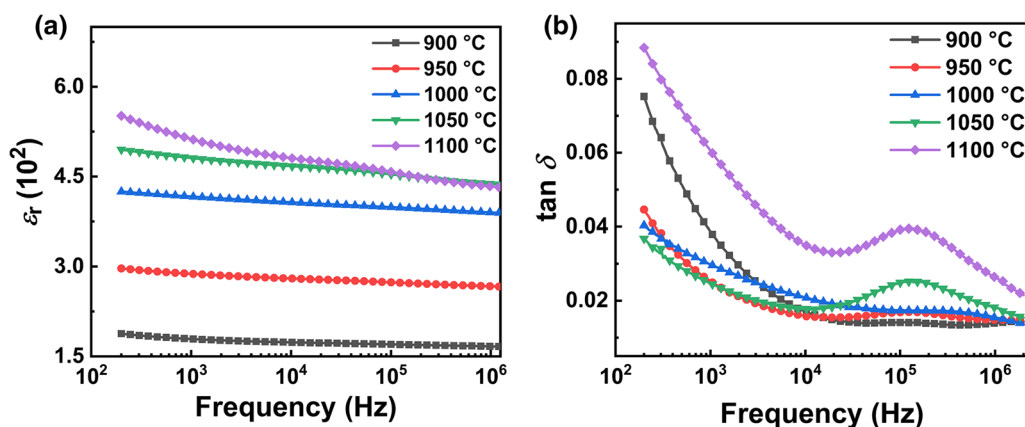


Fig. 7 The microstructural evolution of the ZnO varistors with increasing sintering temperature.





**Fig. 8** Relative dielectric constant (a) and loss tangent (b) as a function of frequency for the ZnO varistors obtained at different temperatures.

of  $43.4 \pm 2.3$ , a voltage gradient of  $451 \pm 4$  V/mm, and leakage current of  $4.5 \pm 0.4$   $\mu\text{A}/\text{cm}^2$ .

The relative dielectric constant–frequency and loss tangent–frequency curves for the ZnO varistors sintered at different temperatures are shown in Fig. 8. The relative dielectric constant  $\epsilon_r$  increases with increasing temperature overall. Meanwhile, the relative dielectric constant  $\epsilon_r$  decreases only slightly with increasing frequency for the samples obtained at 900–1000°C and then decreases near the frequency of 0.15 MHz for samples obtained at 1050°C and 1100°C, corresponding to the loss peaks shown in Fig. 8b. This is due to the electronic relaxation polarization from the intrinsic oxygen vacancies and zinc interstitial defects.<sup>35</sup> It reveals that ion diffusion is stronger for the sample sintered at higher temperature, leading to more obvious polarization and loss peak. The loss tangent  $\tan\delta$  is less than 0.04 in the frequency range of 200 Hz to 2 MHz for the sample sintered at 1000°C.

## Conclusion

The effect of sintering temperature on the microstructural evolution and electrical properties of ZnO-Bi<sub>2</sub>O<sub>3</sub>-Sb<sub>2</sub>O<sub>3</sub>-MnO<sub>2</sub>-Co<sub>2</sub>O<sub>3</sub>-Cr<sub>2</sub>O<sub>3</sub>-SiO<sub>2</sub> varistors was studied in detail. With sintering at 900°C, polyhedral Bi-rich phase Bi<sub>3.73</sub>Sb<sub>0.27</sub>O<sub>6.0+x</sub> was distributed in the ZnO grain boundaries, preventing the effective formation of a double Schottky barrier. With an increase in temperature from 900°C to 1000°C, Bi-rich liquid phase dissolving a mass of Sb, Cr, and Mn formed during sintering, and lamellar Bi-rich phase Bi<sub>3.73</sub>Sb<sub>0.27</sub>O<sub>6.0+x</sub> with the beneficiation of Mn and Cr formed in the ZnO grain boundaries during cooling. Excess O and enriched Mn<sup>4+</sup> in Bi-rich phase Bi<sub>3.73</sub>Sb<sub>0.27</sub>O<sub>6.0+x</sub> served as oxidizing agent to accept e<sup>-</sup>, which improved the double Schottky barrier. Therefore, the barrier height increased, the nonlinear coefficient increased, and the

leakage current density decreased with the increase in temperature from 900°C to 1000°C. When the temperature was further increased from 1000°C to 1100°C, the volatilization of Bi-rich phase intensified, and the thickness of the Bi-rich thin layers clearly increased, leading to poorer uniformity of the Bi-rich thin layers. Therefore, the microstructure and electrical properties deteriorated at a sintering temperature higher than 1000°C. The voltage gradient decreased with increasing temperature due to the increased grain size. Ion diffusion was stronger for the sample sintered at higher temperature, leading to more obvious polarization and loss peak. Finally, ZnO varistors sintered at 1000°C for 2 h obtained a nonlinear coefficient of  $43.4 \pm 2.3$ , voltage gradient of  $451 \pm 4$  V/mm, and leakage current density of  $4.5 \pm 0.4$   $\mu\text{A}/\text{cm}^2$ , thus showing optimal microstructural uniformity and reproducibility. The intensive study of sintering temperature has important relevance for the preparation of ZnO varistors with excellent microstructural uniformity and electrical properties.

**Acknowledgments** This work is supported by the National Natural Science Foundation of China (51802183).

**Conflict of interest** The authors declare no conflicts of interest.

## References

1. A.K. Ray, *Oxide Electronics* (New York: Wiley, 2021), p. 157.
2. D.R. Clarke, Varistor ceramics. *J. Am. Ceram. Soc.* 82, 485 (1999).
3. H. Jiang, X. Ren, X. Lao, A. Kong, M. Zhong, Y. Sun, Y. Wu, Z. Yao, and L. Shi, Effect of NiO doping on grain growth and electrical properties of ZnO-based varistors. *J. Eur. Ceram. Soc.* 42, 3898 (2022).
4. P. Meng, S. Gu, J. Wang, J. Hu, and J. He, Improving electrical properties of multiple dopant ZnO varistor by doping with indium and gallium. *Ceram. Int.* 44, 1168 (2018).
5. Y. Zheng, M. Fujimoto, Y. Sato, and S. Yoshikado, Effects of addition of chromium and/or nickel oxides on the electrical

- characteristics of yttrium oxide-doped high-voltage zinc oxide varistors. *J. Eur. Ceram. Soc.* 41, 4841 (2021).
6. S.A.S. Qaid, M.A.A. Issa, A.M. Hassib, B.A. Al-Asbahi, E.M. Abuassaj, and A.A.A. Ahmed, A novel method for improving the microstructure and electrical properties of  $\text{Pr}_6\text{O}_{11}$ -based ZnO varistors. *J. Korean Ceram. Soc.* (2022). <https://doi.org/10.1007/s43207-022-00221-0>.
  7. W. Long, J. Hu, J. Liu, J. He, and R. Zong, The effect of aluminum on electrical properties of ZnO varistors. *J. Am. Ceram. Soc.* 93, 2441 (2010).
  8. H. Zhao, J. Hu, S. Chen, Q. Xie, and J. He, High nonlinearity and high voltage gradient ZnO varistor ceramics tailored by combining  $\text{Ga}_2\text{O}_3$ ,  $\text{Al}_2\text{O}_3$ , and  $\text{Y}_2\text{O}_3$  dopants. *J. Am. Ceram. Soc.* 99, 769 (2016).
  9. W. Long, J. Hu, J. Liu, and J. He, Effects of cobalt doping on the electrical characteristics of Al-doped ZnO varistors. *Mater. Lett.* 64, 1081 (2010).
  10. M. Zhao, W. Cui, Z. Liu, and H. Chen, Effect of  $\text{Bi}_2\text{O}_3$  on the ZnVMnCoTiO based varistor ceramic sintered at 800 °C. *J. Mater. Sci. Mater. Electron.* 32, 19724 (2021).
  11. L. Zhang, J. Gao, W. Liu, Q. Guo, S. Li, and J. Li, Simultaneously enhanced electrical stability and nonlinearity in ZnO varistor ceramics: role of Si-stabilized  $\delta$ - $\text{Bi}_2\text{O}_3$  phase. *J. Eur. Ceram. Soc.* 41, 2641 (2021).
  12. H. Bai, M. Li, Z. Xu, R. Chu, J. Hao, H. Li, C. Chen, and G. Li, Influence of  $\text{SiO}_2$  on electrical properties of the highly nonlinear ZnO- $\text{Bi}_2\text{O}_3$ - $\text{MnO}_2$  varistors. *J. Eur. Ceram. Soc.* 37, 3965 (2017).
  13. K. Cheng, H. Zhao, Y. Zhou, and Q. Xie,  $\text{B}_2\text{O}_3$ - and  $\text{Y}_2\text{O}_3$ -doped ZnO varistor ceramics: enhanced voltage gradient and nonlinear properties for UHV. *Mater. Sci. Semicond. Proc.* 123, 105590 (2021).
  14. K. Hembram, T.N. Rao, R.S. Srinivasa, and A.R. Kulkarni, CaO doped ZnO- $\text{Bi}_2\text{O}_3$  varistors: grain growth mechanism, structure and electrical properties. *Ceram. Int.* 47, 1229 (2021).
  15. J. Niu, H. She, Z. Liu, M. Cheng, J. Xu, J. Liu, G. Chen, B. Tang, and D. Xu, A current-controlled flash sintering processing leading to dense and fine-grained typical multi-element ZnO varistor ceramics. *J. Alloys Compd.* 876, 160124 (2021).
  16. Y. Mei, S. Pandey, W. Long, J. Liu, S. Zhong, L. Zhang, S. Du, and D. Xu, Processing and characterizations of flash sintered ZnO- $\text{Bi}_2\text{O}_3$ - $\text{MnO}_2$  varistor ceramics under different electric fields. *J. Eur. Ceram. Soc.* 40, 1330 (2020).
  17. R.F.K. Gunnewiek, C.P.F. Perdomo, I.C. Cancellieri, A.L.F. Cardoso, and R.H.G.A. Kiminami, Microwave sintering of a nanostructured low-level additive ZnO-based varistor. *Ceram. Int.* 46, 15044 (2020).
  18. J. Liang, X. Zhao, J. Sun, L. Ren, R. Liao, L. Yang, and W. Li, Enhanced electrical properties of ZnO varistor ceramics by spark plasma sintering: role of annealing. *Ceram. Int.* 46, 15076 (2020).
  19. V. Nečina, and W. Pabst, Influence of the heating rate on grain size of alumina ceramics prepared via spark plasma sintering (SPS). *J. Eur. Ceram. Soc.* 40, 3656 (2020).
  20. A. Boumezoued, K. Guergouri, R. Barille, D. Rechem, and Z. Mourad, Synthesis and characterization of ZnO-based nanopowders: study of the effect of sintering temperature on the performance of ZnO- $\text{Bi}_2\text{O}_3$  varistors. *J. Mater. Sci. Mater. Electron.* 32, 3125 (2021).
  21. R.K. Sendi, and A.M. Ali, Dependence of the nonlinear behaviour stability of a ZnO nanoparticle- $\text{Bi}_2\text{O}_3$ - $\text{Mn}_2\text{O}_3$ -based varistor system on cooling rates during ceramic processing. *Microsc. Res. Tech.* 84, 723 (2021).
  22. J. Li, S. Yang, Y. Pu, and D. Zhu, Effects of pre-calcination and sintering temperature on the microstructure and electrical properties of ZnO-based varistor ceramics. *Mater. Sci. Semicond. Process.* 123, 105529 (2021).
  23. Z. Fu, J. He, J. Lu, Z. Fang, and B. Wang, Investigation of dielectric relaxation and degradation behavior of two-step sintered ZnO varistors. *Ceram. Int.* 45, 21900 (2019).
  24. H. Wang, H. Zhao, W. Liang, S. Fan, and J. Kang, Effect of sintering process on the electrical properties and microstructure of Ca-doped ZnO varistor ceramics. *Mater. Sci. Semicond. Process.* 133, 105880 (2021).
  25. C.W. Nahm, Effect of sintering temperature on varistor properties and aging characteristics of ZnO- $\text{V}_2\text{O}_5$ - $\text{MnO}_2$  ceramics. *Ceram. Int.* 35, 2679 (2009).
  26. J. Cai, Y.-H. Lin, M. Li, C.-W. Nan, J. He, and F. Yuan, Sintering temperature dependence of grain boundary resistivity in a rare-earth-doped ZnO varistor. *J. Am. Ceram. Soc.* 90, 291 (2007).
  27. C.W. Nahm, The effect of sintering temperature on varistor properties of (Pr Co, Cr, Y, Al)-doped ZnO ceramics. *Mater. Lett.* 62, 4440 (2008).
  28. S.-N. Bai, and T.-Y. Tseng, Influence of sintering temperature on electrical properties of ZnO varistors. *J. Appl. Phys.* 74, 695 (1993).
  29. X.-Y. Wu, J.-R. Liu, Y. Chen, and M.-H. Wang, Effect of  $\text{B}_2\text{O}_3$  concentration and sintering temperature on microstructure and electrical properties in the ZnO- $\text{Bi}_2\text{O}_3$ -based varistors. *J. Electron. Mater.* 48, 7704 (2019).
  30. J. Liu, Z. Li, S. Liu, R. Xu, J. Chen, J. Su, L. Li, and W. Cao, The influence of sintering temperature on the structure and electrical properties of ZBCMS varistors. *J. Mater. Sci.-Mater. Electron.* 33, 12104 (2022).
  31. P.R. Bueno, J.A. Varela, and E. Longo,  $\text{SnO}_2$ , ZnO and related polycrystalline compound semiconductors: an overview and review on the voltage-dependent resistance (non-ohmic) feature. *J. Eur. Ceram. Soc.* 28, 505 (2008).
  32. F. Cui, Z. Xu, R. Chu, X. He, X. Guo, and G. Li, Low temperature sintering ZnO- $\text{Bi}_2\text{O}_3$  based varistor ceramics with low electrical breakdown voltage and high nonlinear coefficient. *Ceram. Int.* 47, 4118 (2021).
  33. W. Cao, X. Xie, Y. Wang, M. Chen, Y. Qiao, P. Wang, Y. Zhang, and J. Liu, Effect of  $\text{Pr}_6\text{O}_{11}$  Doping on the microstructure and electrical properties of ZnO varistors. *Ceram. Int.* 45, 24777 (2019).
  34. M. Guo, X. Zhao, W. Shi, B. Zhang, K. Wu, and J. Li, Simultaneously improving the electrical properties and long-term stability of ZnO varistor ceramics by reversely manipulating intrinsic point defects. *J. Eur. Ceram. Soc.* 42, 162 (2022).
  35. L. Zhang, W. Liu, J. Gao, F. Kong, Y. Li, and S. Li, Effects of the  $\text{Er}_2\text{O}_3$  doping on the microstructure and electrical properties of ZnO- $\text{Bi}_2\text{O}_3$  based varistor ceramics. *Ceram. Int.* 47, 32349 (2021).
  36. J. Bernasconi, H.P. Klein, B. Knecht, and S. Strässler, Investigation of various models for metal oxide varistors. *J. Electron. Mater.* 5, 473 (1976).
  37. B. Cui, J. Niu, P. Peng, L. Shi, S. Du, J. Liu, and D. Xu, Flash sintering preparation and electrical properties of ZnO- $\text{Bi}_2\text{O}_3$ -M (M =  $\text{Cr}_2\text{O}_3$ ,  $\text{MnO}_2$  or  $\text{Co}_2\text{O}_3$ ) varistor ceramics. *Ceram. Int.* 46, 14913 (2020).
  38. K. Mukae, K. Tsuda, and I. Nagasawa, Capacitance-vs-voltage characteristics of ZnO varistors. *J. Appl. Phys.* 50, 4475 (1979).

**Publisher's Note** Springer Nature remains neutral with regard to jurisdictional claims in published maps and institutional affiliations.

Springer Nature or its licensor (e.g. a society or other partner) holds exclusive rights to this article under a publishing agreement with the author(s) or other rightsholder(s); author self-archiving of the accepted manuscript version of this article is solely governed by the terms of such publishing agreement and applicable law.